International Journal of Fluid Machinery and Systems
Vol. 2, No. 4, October-December 2009

Original Paper

Experimental Study on Surge Inception in a Centrifugal Compressor

Hideaki Tamaki

Turbo Machinery and Engine Technology Department
IHI Corporation
1, Shin-nakahara-cho, Isogo-ku, Yokohama, 235-8501, Japan

Abstract

An investigation of surge inception in a centrifugal compressor was done with measurements of steady and unsteady static pressure. Vaneless diffuser and vaned diffuser were tested. Analyses of the static pressure and the pressure fluctuation showed that stall at the impeller leading edge occurred at first, and then it extended to downstream. In case of the vaneless diffuser, deterioration of the pressure rise in the impeller triggered instability. For the vande diffuser, instability that was generated in the impeller propagated into the vaned diffuser, however the pressure recovery by the vaned diffuser made the operation of the compressor stable at low flow rate.

Keywords: Centrifugal Compressor, Surge, Pressure Fluctuation, Vaned Diffuser

1. Introduction

A turbo-compressor is operated within the limited flow range. Maximum flow is determined by choking at some element of the compressor system. As mass flow is reduced, a breakdown of stable flow conditions, rotating stall and surge, occur. Minimum flow is determined by this instability. Flow instability, particularly surge, causes not only the deterioration of compressor performance, but also mechanical damage due to dynamic excitations. If prediction and control of the inception of rotating stall and surge are possible, one can design a compressor without substantially sacrificing performance. Numerous works have been done on rotating stall and surge for compressors, axial compressors particularly. For example, the process leading to the formation of finite amplitude rotating stall cells has been extensively studied experimentally and numerically [1-3]. It is said that two types of rotating stall inception occur in axial compressors. One is long-length-scale disturbance referred to as modal inception and another is short-length disturbance known as "spike". The concept of using rotating stall control to increase the stable operating range is vigorously investigated as well. Many results of applications of rotating stall controlling devices to research compressors and gas turbine engines have been demonstrated [4-5]. However, compared to axial compressors, relatively little data is available in literature about flow instability in centrifugal compressors. Experimental results and correlations are still of great importance to understand stall and surge in centrifugal compressors accordingly.

2. Experimental Apparatus

Fig. 1 shows the schematic view of a tested centrifugal compressor. Impeller main dimensions and tested rotational speed were

Impeller Outer Radius (R_2)	123.5 mm	Impeller Exit Width	12.8 mm
Backward Angle at Impeller Exit	30°	Rotational Speed	24178 rpm
Number of Blades (full/splitter)	20(10/10)		

Pressure measurement taps were located at station ①, ② and ③ along the impeller shroud. Station ① was at $0.02m_2$, 2mm downstream from the impeller leading edge. Station ② and ③ were $0.42m_2$ and $0.53m_2$, 0.6mm and 10.6mm downstream from the splitter leading edge respectively. m_2 is a meridional length at shroud measured from the leading edge of the impeller.

Vaneless diffuser and vaned diffuser were tested. Pressure measurement taps were located at the impeller radius ratio of 1.07, 1.15 and 1.58 for the vaneless diffuser. Fig. 2 shows the tested vaned diffuser and positions of the pressure measurement taps along the centerline between vanes. The uncertainty of pressure ratio was 0.5% and flow rate was 0.7%. The main dimensions of the vaned diffuser were

Received September 2 2009; accepted for publication September 22 2009: Review conducted by Prof. Zhang Yangjun. (Paper number O09038)
Corresponding author: Hideaki Tamaki, Dr., hideaki_tamaki@ihi.co.jp

Number of Vanes	19		
Position of Leading Edge	1.15 R_2	Vane Setting Angle at Leading Edge	68°
Position of Trailing Edge	1.56 R_2	Vane Setting Angle at Trailing Edge	52°

Unsteady pressure measurements with semiconductor pressure transducers (Kulite XCQ-062, natural frequency 500 kHz) were done at station ①, ②, ③ and ④. The pressure transducers installed at ①, ② and ③ were calibrated with a pressure gauge tester. The pressure transducers were nearly flush-mounted on the shroud or hub wall. Rotational speeds were measured with an optical sensor. In case of the test with the vaneless diffuser, velocity fluctuation upstream of the impeller was measured with a hot wire probe (Dantec, 55P01). The position of the hot wire probe was at 48% of the axial blade length of the impeller from its leading edge.

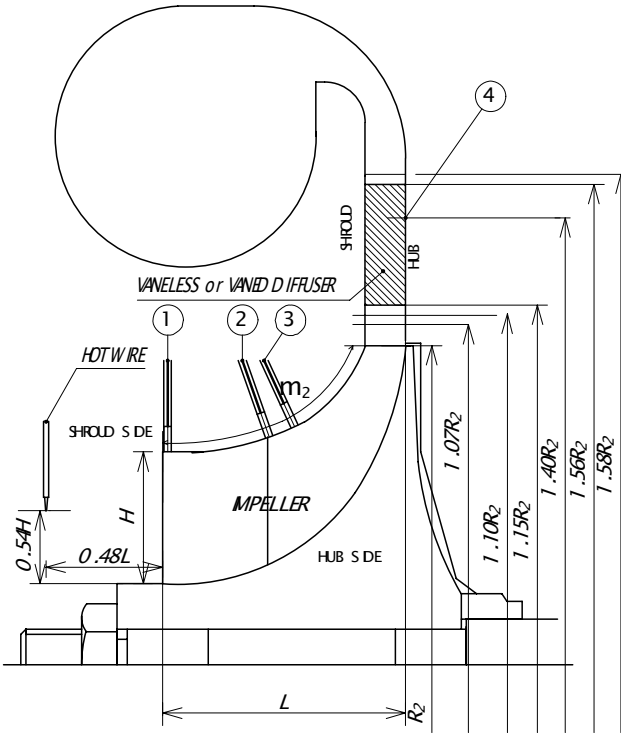

Fig. 1 Schematic of Tested Centrifugal Compressor

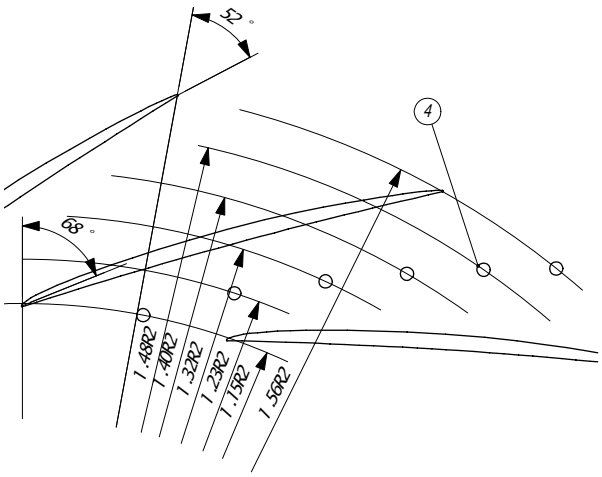

Fig. 2 Tested Vaned Diffuser

3. Experimental Results and Discussions

3.1 Compressor with Vaneless Diffuser

3.1.1 Performance of Centrifugal Compressor

Ratio of total pressure at the compressor inlet to static pressure is shown in Fig. 3. Fig. 3 includes the static pressure not only at the scroll exit, corresponds to the compressor exit, but also at ①, ②, ③, R/R_2=1.07, 1.10 1.15 and 1.58. Q is the ratio of mass flow rate to a reference mass flow rate. As mass flow is reduced, the static pressure at ①, ② and ③ takes maximum value before the static pressure at the scroll exit reaches maximum value. ② and ③ take the maximum static pressure at the flow rate 'ia' (Q=0.83) that is smaller than the flow rate 'h' (Q=0.87) at which the maximum static pressure at ① is. It is assumed that stall occurred at the leading edge at first, and then stall region extended to downstream. According to the static pressure at R/R_2=1.07, the maximum static pressure rise in impeller is assumed at 'j' (Q=0.78). The flow rate at which the static pressure at the scroll exit reaches maximum value is 'j' (Q=0.78), and it is 91% of the flow rate at which the static pressure at ① takes maximum value.

Fig. 4 shows the velocity fluctuations upstream of the impeller and their frequency spectrum. No remarkable peak of frequency is found up to 'ia' (Q=0.83). Remarkable peak of 13Hz appears at the flow rate 'ka' (Q=0.74) and hence the flow rate 'j' (Q=0.78) at which the static pressure at the scroll exit reaches maximum value is assumed to be the minimum flow rate where the tested compressor can be operated stably.

Fig. 5 shows performance of another compressor (called A-compressor here). A-compressor used the tested vaneless diffuser and scroll. A-compressor installed the impeller whose difference from the tested impeller was only the shape of splitter leading edge [6]. Characteristics of A-compressor are considered to be similar to the tested compressor accordingly. Fig. 5 shows total-to-total pressure ratios at scroll exit of A-compressor with and without casing treatment, and also includes the tested compressor performance. Application of the casing treatment to the impeller is able to shift minimum stable flow rate toward low flow rate. Hence, it seems reasonable to think that the impeller characteristics of the tested compressor control the compressor operating range. A vaneless diffuser is known as an unstable component for a centrifugal compressor essentially, because the friction loss in vaneless diffuser increases as the flow rate decreases [7]. In this case, the pressure rise in an impeller makes operation of a centrifugal compressor stable, and hence the deterioration of the pressure rise in the impeller determines the minimum stable flow rate.

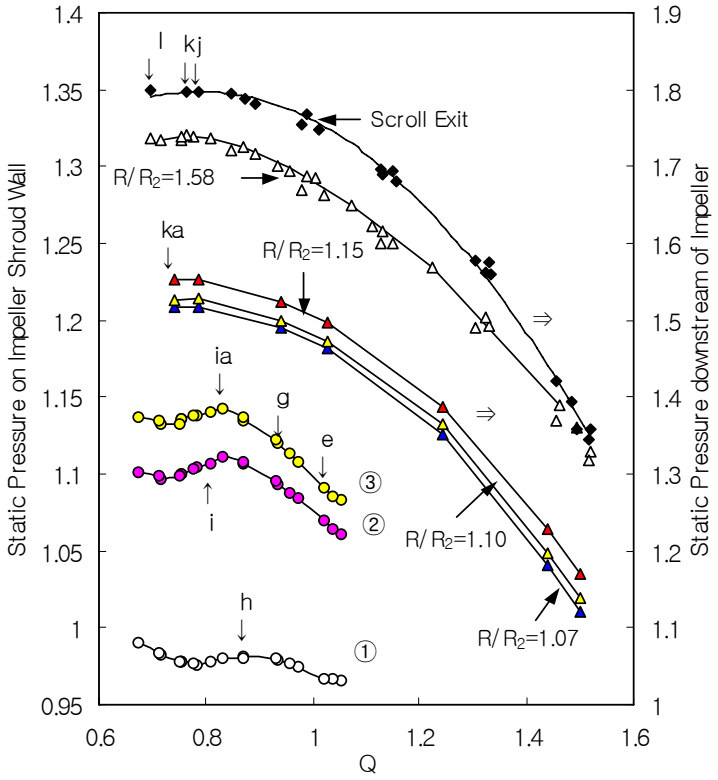

Fig. 3 Static Pressure Ratio in Compressor with Vaneless Diffuser

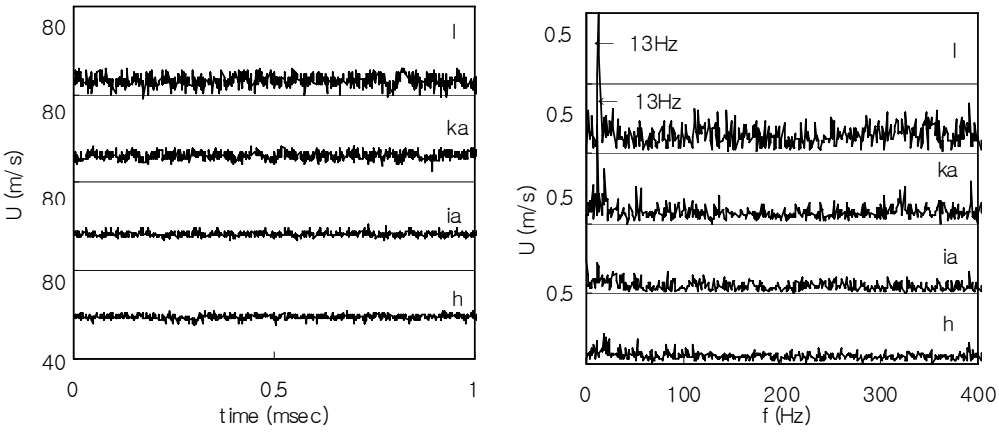

Fig. 4 Velocity Fluctuation Upstream of Impeller

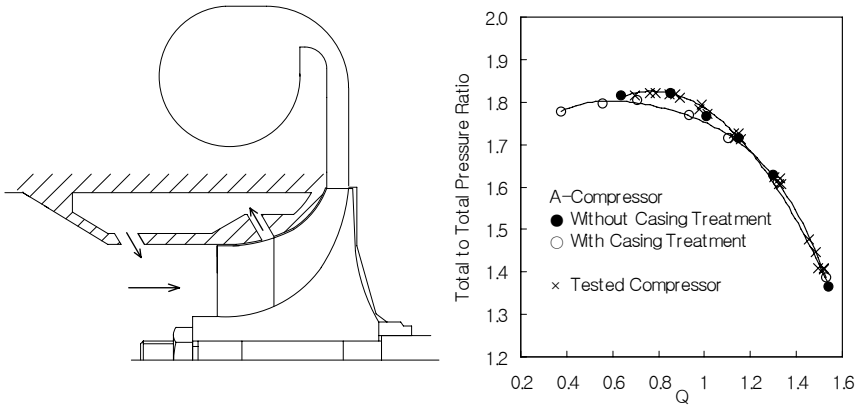

Fig. 5 Compressor Performance

3.1.2 Measurement of Static Pressure Fluctuation

Fig. 6 shows the signals of the pressure transducers at ①, ② and ③. Sampling time was 10μs. The periodicity of the wave at ① is disturbed at the flow rate 'h' (Q=0.87) and the periodicities of the waves at ② and ③ are disordered at the flow rate 'i' (Q=0.81). These signals were sampled periodically and the static pressure change in a pitch of the blade was derived with the following way. Δt that is the time required for one pitch of full blade to pass a pressure measurement tap is

$$\Delta t = 60/(Z_f N)$$

Z_f corresponds to the number of full blade and N (rpm) is the rotational speed. When the static pressure change in one pitch of the full blade is interpolated with the number of data of M, T_{ij} that is the time for the position of No. i (i =1 to M) to pass the static pressure measurement tap is

$$T_{ij} = (\Delta t / M) \cdot i + \Delta t \cdot j \qquad (j = 1 \ \ to \ \ j_{\max})$$

jmax is the maximum number which satisfies the condition $T_{ij} \leqq T_m$. Tm is total measurement time. The average pressure at the number of the position 'i', P_i, is

$$P_i = \sum_{j=1}^{j=j_{\max}} P_{ij} / j_{\max}$$

P_{ij} is the static pressure of the position of No. i at T_{ij}. In order to observe instability of the static pressure, present study defined the deviation between the time averaged and the instantaneous static pressure in one pitch of blade σ_i, as follows.

$$\sigma_i = \sqrt{\sum_{j=1}^{j=j_{\max}} (P_{ij} - P_i)^2 / j_{\max}}$$

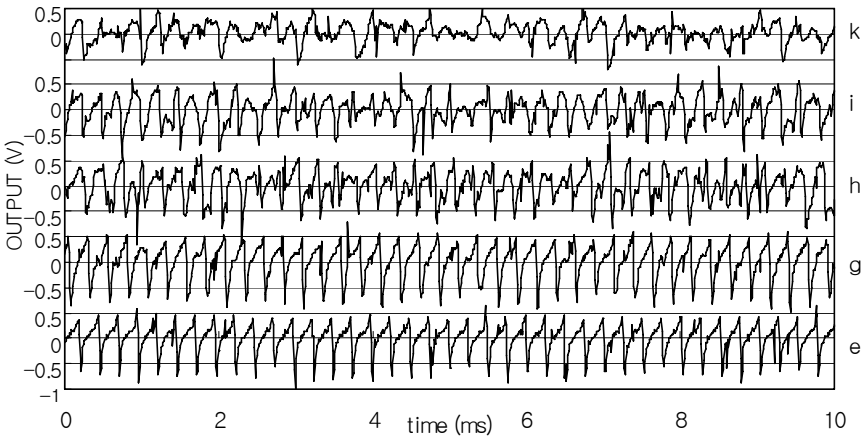

Fig. 6(a) Signal of Pressure Transducer at ①

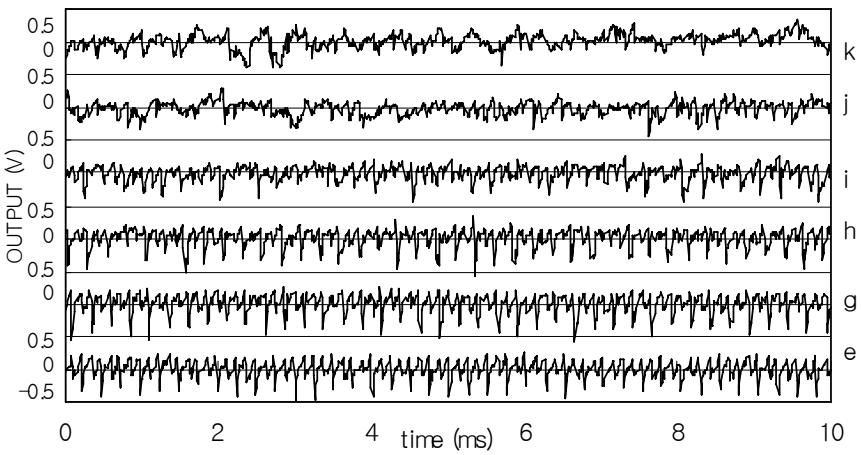

Fig. 6(b) Signal of Pressure Transducer at ②

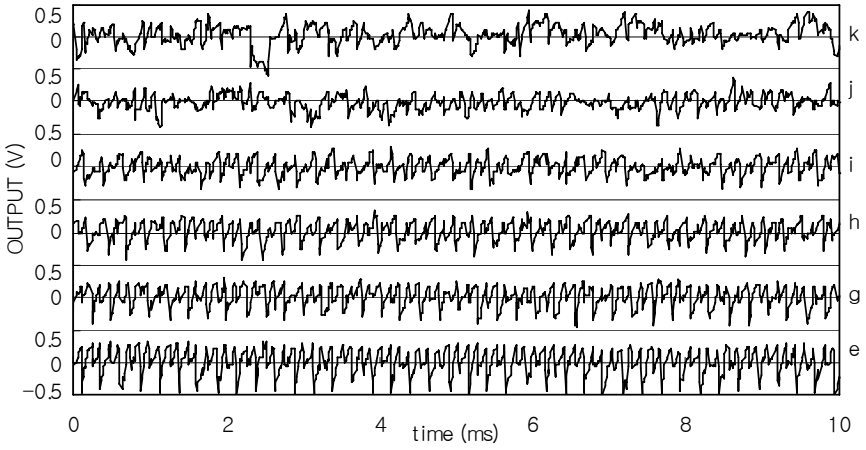

Fig. 6(c) Signal of Pressure Transducer at ③

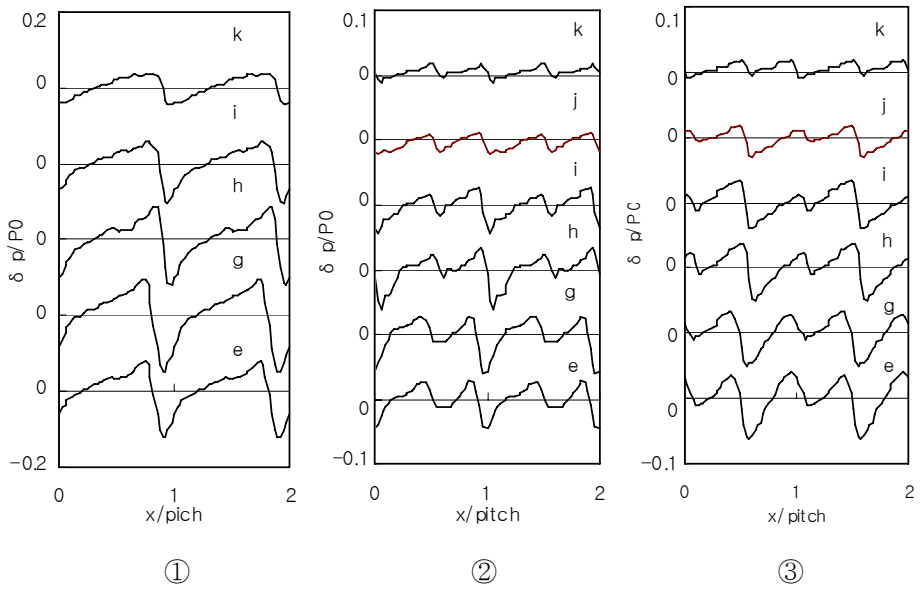

Fig. 7 Static Pressure Change in a Pitch of Blade

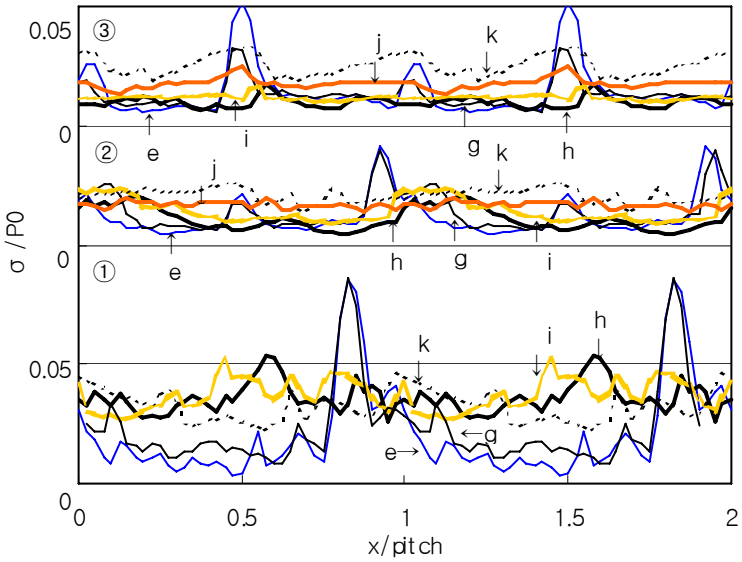

Fig. 8 Static Pressure Change in a Pitch of Blade

Fig. 7 shows the static pressure change in one pitch of full blade. The deviation, σ_i, is shown in Fig. 8. Ordinates 'δ_p/P0' and 'σ/P0' are ratios of total pressure at the compressor inlet, P0, to static pressure change and to deviation respectively. 'pitch' in the abscissa is a length of one pitch of the full blade. Irregularities on the curve of the static pressure change at ① and ② appear

at ‘h’ (Q=0.87). The deviation, σ_i, at ① start to increase all over the pitch at ‘h’ (Q=0.87). The flow rate at that σ_i at ② and ③ start to increase all over the pitch is ‘j’ (Q=0.78). The results of the frequency analyses are shown in Fig. 9. The dominant frequencies are observed at harmonics and subharmonics of the blade passing frequencies at each flow rate. The low frequency component appears at ‘h’ (Q=0.87) at ①, at ‘i’ (Q=0.81) at ② and ‘j’ (Q=0.78) at ③. According to above results, flow instability occurs at ‘h’ (Q=0.87) at ①, among ‘h’ and ‘j’ (Q=0.87 to 0.78) at ② and at ‘j’ (Q=0.78) at ③. This result shows that stall region extended from the leading edge to downstream as discussed in the previous section and that it would be possible to detect the inception of instability, which limited the compressor operation, by monitoring the deviation, σ_i, at the latter part of impeller. This study defines stall at the impeller leading edge as the inducer stall.

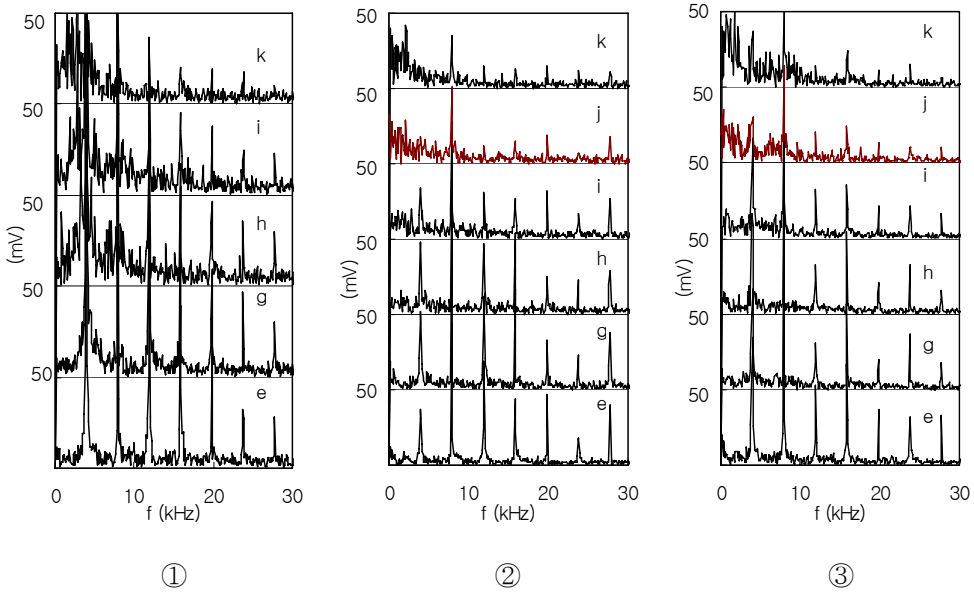

Fig. 9 Frequency Spectrum

3.2 Compressor with Vaned Diffuser

3.2.1 Performance of Centrifugal Compressor

Ratio of total pressure at the compressor inlet to static pressure with the vaned diffuser is shown in Fig. 10. Fig. 10 shows the static pressure at the scroll exit, R/R_2=1.15,1.23, and 1.56. Fig. 10 also includes the static pressure at ①, ②, ③, R/R_2=1.07 and 1.15 in Fig. 3. The flow rate where the static pressure at scroll exit takes maximum value is ‘lva’ (Q=0.68), which is 78% of the flow rate at the inducer stall, ‘h’ (Q=0.87). Since ‘lva’ (Q=0.68) is 86% of the minimum stable flow rate for the vaneless diffuser test, the vaned diffuser characteristics could be the key to the unstable operation of the compressor.

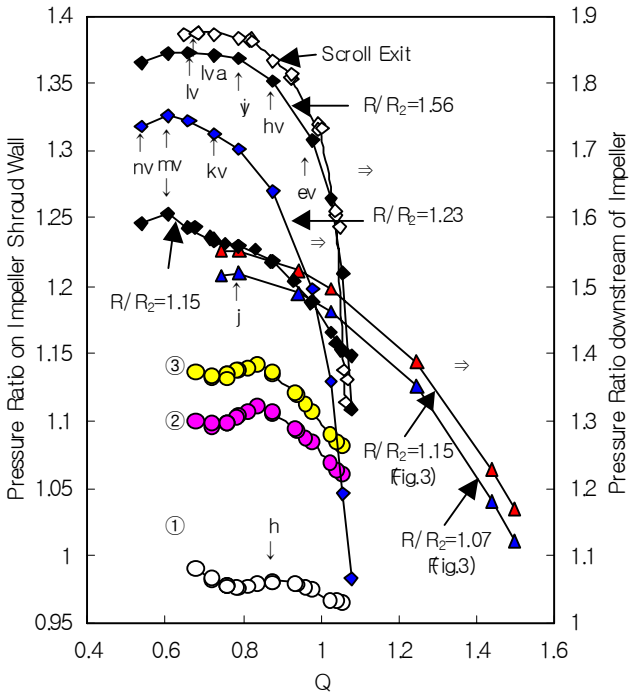

Fig. 10 Static Pressure in Compressor with Vaned Diffuser

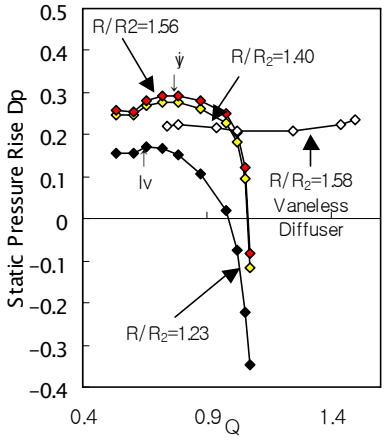

Fig. 11 Static Pressure Rise

The maximum static pressure at R/R_2=1.15 for the vaneless diffuser is at 'j' (Q=0.78) in Fig. 3 and that for the vaned diffuser is at 'mv' (Q=0.61). Although the static pressure at the impeller exit decreases as the flow is reduced below 'j' (Q=0.78), the flow turning by the vaned diffuser increases the static pressure downstream of the impeller. As the result, the static pressure at the scroll exit increases up to 'lva' (Q=0.68), when the flow decreases.

The maximum static pressure at R/ R_2=1.56, the vaned diffuser exit, is at 'lv' (Q=0.66) and that at R/ R_2=1.23 is at 'mv' (Q=0.61). In general, the pressure recovery in the semi-vaneless space that corresponds to the portion from the leading edge of the vaned diffuser to the throat increases, as the flow decreases, due to the increase of the diffusion. This increase of the pressure recovery thickens the boundary layers at the throat, and consequently, the blockage at the throat increases. The effect of this increased throat blockage is to reduce the pressure recovery of the passage portion that is the position from the throat to the vaned diffuser exit. Overall pressure recovery is combination of the pressure recovery in the semi-vaneless space with that in the passage portion. Hence the pressure recovery of the vaned diffuser begins to decrease below a certain flow rate, as the flow rate is reduced. This is the reason why the flow rate, where the maximum static pressure is, changes at the different position in the vaned diffuser.

Fig. 11 shows the static pressure rise in the vaned diffuser. The static pressure rise in vaneless diffuser is also included. Dp is the pressure rise from R/ R_2=1.15 to a certain position in the diffuser divided by the square of the peripheral speed. In case of the vaned diffuser, the maximum Dp from R/ R_2=1.15 to R/ R_2=1.23 is at 'lv' (Q=0.66) and from R/ R_2=1.15 to R/ R_2=1.40 and R/ R_2=1.56 is at 'jv' (Q=0.79). This different is also due to the effect of the thickness of the throat blockage.

3.2.2 Measurement of Static Pressure Fluctuation

Fig. 12 and Fig. 13 show the signals of the pressure transducers at ③ and ④. The sampling time of Fig. 12 is 10μs and that of Fig. 13 is 2ms. Although the signals at ① and ② are not presented here, the periodicities of the waves with the sampling time of 10μs show the same tendency as those in Fig. 6. Since the signal at ④ in Fig. 12 (b) is similar to that at ③ in Fig. 12 (a), instability occurred in the impeller propagates into the diffuser. Fig. 14 shows the signals of the pressure transducers at ①, ②, ③ and ④ at 'nv' (Q=0.54). At about 1.6 sec, the signal ④ rises and the increase of the signals at ② and ③ follows. Hence the vaned diffuser is assumed to be a trigger of surge.

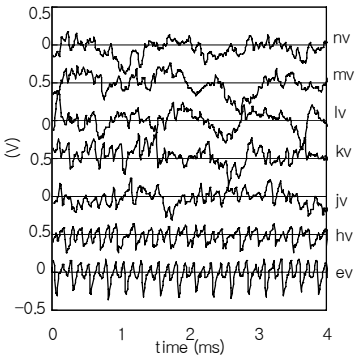

Fig. 12(a) Signal of Transducer ③

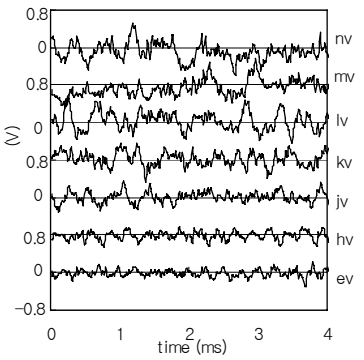

Fig. 12(b) Signal of Transducer ④

The results of the frequency analyses of the signals with the sampling time of 2ms are shown in Fig. 15. The dominant frequencies are observed at 83Hz and 166Hz at the stable operating point, 'ev' (Q=0.98). The reason why these frequencies appear is unclear, but those might be due to the interaction between the impeller and the diffuser vanes. As the flow rate is reduced, these oscillations become weaker and disappear. As the flow rate is reduced further, the peak frequency of 9.3Hz appears at 'mv' (Q=0.61) except ① and at 'nv' (Q=0.54) for all the positions. The peak of frequency at 'mv' (Q=0.61) is the same as that at 'nv' (Q=0.54). In case of the test with the vaned diffuser, the impeller is operated unstably at the low flow rate, while the pressure rise in the vaned diffuser suppresses this instability.

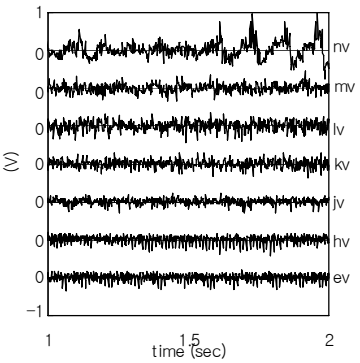

Fig. 13(a) Signal of Transducer ③

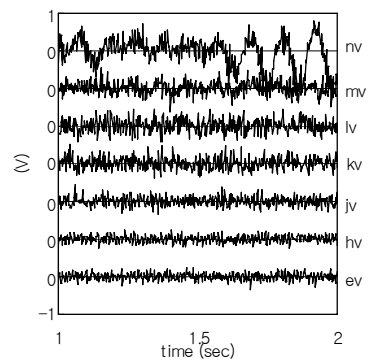

Fig. 13(b) Signal of Transducer ④

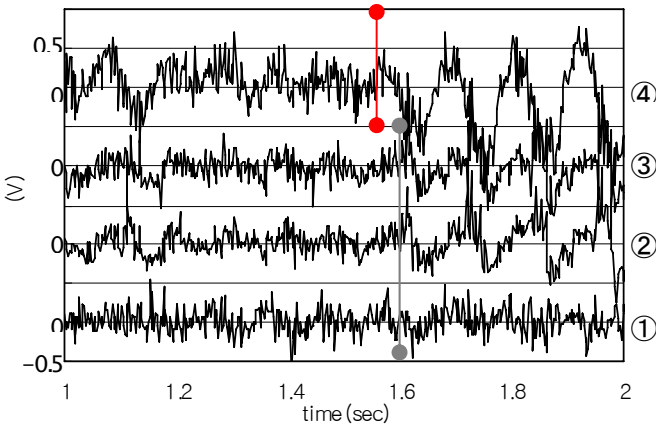

Fig. 14 Signal of Transducers at 'nv'

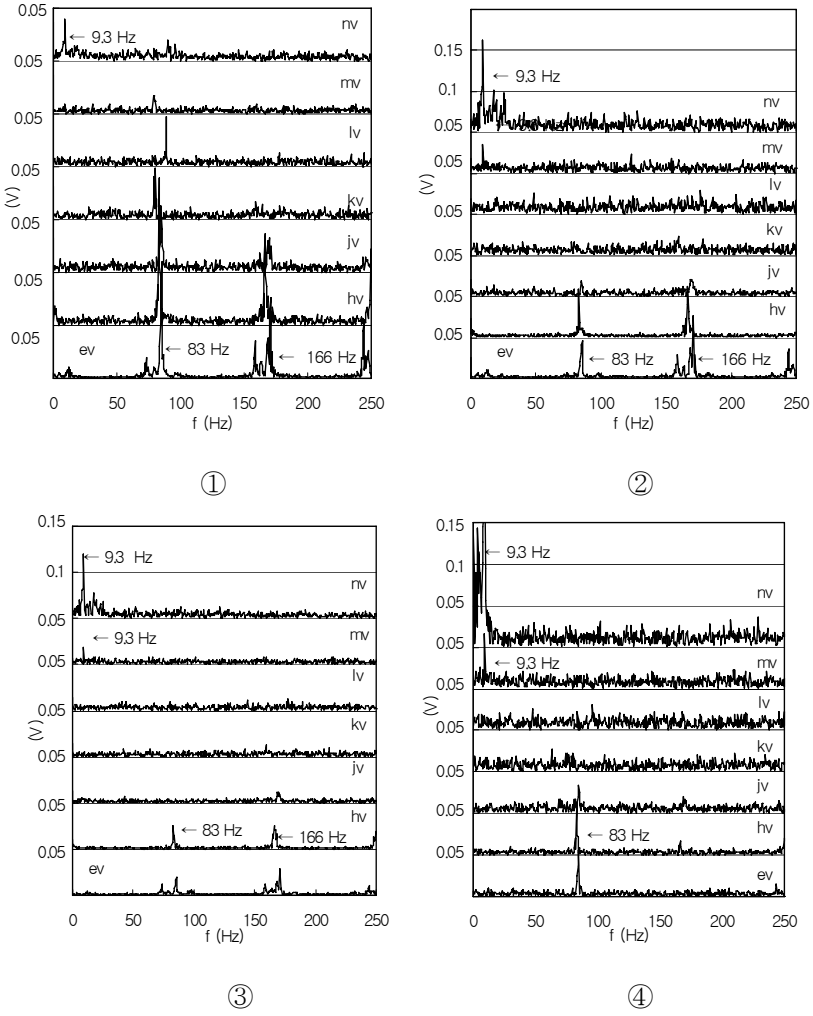

Fig. 15 Frequency Spectrum

4. Conclusion

The investigation of surge inception in the centrifugal compressor was done with the measurements of steady and unsteady static pressure.

In case of the vaneless diffuser, stall in the impeller was key to the unstable operation. The test results showed that stall at the impeller leading edge occurred at first, and then stall region extended to the impeller exit. Minimum operating flow rate was 91% of the flow rate at the inducer stall. Since the impeller stall is directly related to flow instability, monitoring the deviation σ_i at the latter part of the impeller is useful to detect the inception of instability which limits the compressor operation.

In case of the vaned diffuser, the flow rate at surge was 86% of the minimum stable flow rate for the vaneless diffuser. Although instability that occurred in the impeller propagated into the vaned diffuser, the pressure rise in the vaned diffuser made the operation of the compressor stable at low flow rate. According to signals of the pressure transducers, the pressure drop in vaned diffuser is assumed to be a trigger of surge.

References

[1] Day, I. J., 1993, "Stall Inception in Axial Compressors," ASME Journal of Turbomachinery, Vol. 115, No. 1, pp. 1-9.
[2] Hoying, D. A., Tan, C. S., Huu Duc, Vo., and Greitzer, E. M., 1999, "Role of Blade Passage Structures in Axial Compressor Rotating Stall Inception," ASME Journal of Turbomachinery, Vol. 121, No. 4, pp. 735-742.
[3] Inoue, M., Kuromaru, M., Tanino, T., and Furukawa, M., 2000, "Propagation of Multiple Short-Length-Scale Stall Cells in an Axial Compressor Rotor," ASME Journal of Turbomachinery, Vol. 122, No. 1, pp. 43-54.
[4] Gysling, D. L., and Greitzer, E. M., 1995, "Dynamic Control of Rotating Stall in Axial Flow Compressor using Aeromechanical Feedback," ASME Journal of Turbomachinery, Vol. 117, No. 3, pp. 307-319.
[5] Freeman, C., Wilson, A. G., Day, I. J., and Swinbanks, M. A., 1998, "Experiments in Active Control of Stall on an Aeroengine Gas Turbine," ASME Journal of Turbomachinery, Vol. 120, No. 4, pp. 637-647.
[6] Tamaki, H., Yamaguchi S., Nakao H., Ishida K., Mitsubori K., 1998, “Development of Compressor for High Pressure Ratio Turbocharger,” IMechE C554/002.
[7] Tamaki, H., Yamaguchi, S. 2007, “The Experimental Study on Matching between Centrifugal Compressor Impellers and Vaneless Diffusers for Turbochargers,” ASME Turbo Expo 2007, Montreal, Canada, GT2007-28300